Standard target calibration

Atkins, P. R.; Yan, T.; Hayati, F.

DOI:
10.1109/OCEANSE.2017.8084801

Standard Target Calibration: Practical inter-comparison with planar surface targets and calibrated transducers

P.R. Atkins T. Yan and F. Hayati
Department of Electronic, Electrical and Systems Engineering
University of Birmingham
Birmingham, United Kingdom
p.r.atkins@bham.ac.uk

***Abstract*— This contribution presents the inter-comparison of three different methods for obtaining amplitude and phase correction functions for broadband transducers used within an experimental scientific echo sounder. The standard target method is compared to the use of a planar boundary and a conventional calibrated PVDF membrane hydrophone. These correction functions enabled a fully corrected scientific active sonar system to be deployed for measuring the statistical repeatability of a production run of standard target spheres using low cost materials such as aluminum. Previous experience had shown that the acoustic characteristics of aluminum stock differed from billet-to-billet and even within a billet. Thus a laboratory method of establishing the efficacy of low-cost standard targets was developed.**

Keywords—active sonar calibration; standard target

I. Introduction

Scientific echo sounders require frequent *in situ* calibration to a high level of repeatability. Total system calibration is required to address changes resulting from aging characteristics of the transducers [1], material interaction with the medium (corrosion and entrapped bubbles) and general variations within the electronic system. Such calibrations are frequently addressed using the standard target process where a passive object of known target strength is deployed within the beam of the scientific echo sounder. Standard targets are frequently spherical to remove angular dependency and are manufactured from materials such as tungsten-carbide, copper or aluminum. It is normally assumed that the material properties of the standard target are known with sufficient accuracy that analytic models can be used to predict the target strength at any operating frequency and selected transmission signal [2].

Of interest to the authors is the application area where simple, low-cost, broad-band sonar systems are deployed on very small vessels such as canoes or AUVs for use within in-shore areas. Such sonars systems would still need to be regularly calibrated in order to be of scientific use [3], but the traditional precision deployment techniques used on research vessels would be infeasible. An alternative might be to mark the perimeter of the survey area with a large number of bottom-tethered standard target spheres. This might provide two advantages: the ability to repeatedly precision navigate within the survey area and to implement fly-by calibration as part of the survey post-processing. Such an approach would require the availability of a large number of low-cost standard targets with closely matched target strengths. Aluminum was an ideal candidate material for the spheres given the claimed consistency of manufacture of the billets and the relatively low density would simplify the deployment process. However, previous experience had shown that the acoustic characteristics of aluminum stock differed from billet-to-billet and even within a billet and no measurements had been conducted to quantify these effects within a laboratory environment.

II. Sonar System Signal Flow Chain

A typical sonar system signal flow chain may take the form shown in Fig. 1. A continuous-time representation of a transmit signal waveform, $s_{TX}(t)$, may be modified by a transmission correction function, $h_{TX}(t)$, prior to being amplified and applied to a projector via a matching circuit. The resulting acoustic signal is subjected to a two-way transmission loss, $h_{2TL}(t)$, and the echo formation process resulting from the interaction with a standard target, $h_{ST}(t)$. The receiver gain and filtering functions will be followed by a receiver correction function, $h_{RX}(t)$, the resulting signal, $s_{RX}(t)$, being the desired compensated received signal. The many individual transfer functions associated with the projector, hydrophone, gain and filtering blocks are lumped together under the term, $h_{SYS}(t)$ and this is the desired parameter resulting from the majority of scientific echo sound calibration procedures. From the viewpoint of standard target manufacture, the establishment of $h_{ST}(t)$ is the desired outcome.

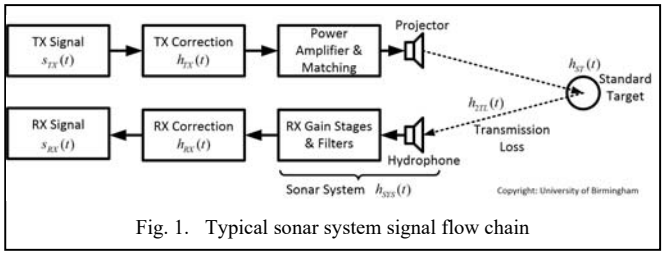

Fig. 1. Typical sonar system signal flow chain

The requirement is to obtain the combined correction function for scientific echo sounder calibration procedures, $h_{TXRX} = h_{TX}(t) \otimes h_{RX}(t)$, representing the convolution of the transmit and receive correction functions. These terms have been deliberately separated to allow the designer to modify the spectral content of the projected signal given knowledge of the ambient noise spectra. The process of obtaining the correction factors may take place in two stages for some sonar systems. The first stage might be to temporarily deploy a broad-band non-resonant sense hydrophone and to adapt $h_{TX}(t)$ to provide a specified acoustic signal in the water. The second stage might be to activate the operational hydrophone and adapt $h_{RX}(t)$ to provide a specified receiver system response. Similarly, the correction factor may be required for multiple hydrophone elements of a transducer array. This process would normally require full knowledge of the physical location of the assumed phase-centers of the array elements and of the standard target.

Alternatively, the combined correction function, h_{TXRX}, may be all that is required and obtained directly using the standard target method.

The continuous-time received signal may defined as:

$$s_{RX}(t) = s_{TX}(t) \otimes h_{TX}(t) \otimes h_{2TL}(t) \otimes h_{ST}(t) \otimes h_{SYS}(t) \otimes h_{RX}(t) \quad (1)$$

It is assumed that $s_{TX}(t)$, $h_{2TL}(t)$ and $s_{RX}(t)$ are known, whilst $h_{TX}(t)$, $h_{RX}(t)$ and $h_{SYS}(t)$ are to be derived via deconvolution. The deconvolution operation is most easily implemented by transforming all quantities to the frequency domain via the transform relationship $s(t) \leftrightarrow S(\omega)$. Thus (1) can be expressed as a frequency domain equivalent:

$$S_{RX}(\omega) = S_{TX}(\omega)\, H_{TX}(\omega)\, H_{2TL}(\omega)\, H_{ST}(\omega)\, H_{SYS}(\omega)\, H_{RX}(\omega) \quad (2)$$

Re-arranging to obtain the correction factors and system transfer function

$$H_{TX}(\omega)\, H_{SYS}(\omega)\, H_{RX}(\omega) = \frac{S_{RX}(\omega)}{S_{TX}(\omega)\; H_{2TL}(\omega)\, H_{ST}(\omega)} \quad (3)$$

A fully corrected sonar system would imply

$$H_{TX}(\omega)\, H_{SYS}(\omega)\, H_{RX}(\omega) \equiv 1, \quad (4)$$

or

$$H_{TX}(\omega)\;\; H_{RX}(\omega) \equiv \frac{1}{H_{SYS}(\omega)}. \quad (5)$$

This would be equivalent to

$$H_{TXRX}(\omega) \equiv \frac{1}{H_{SYS}(\omega)} \quad (6)$$

should a single combined compensation factor be required.

In practical applications, correction will not be possible at frequencies associated with a poor received signal-to-noise ratio. Thus, determining signal-to-noise ratios *in situ* will be key to the correction process.

In use, a compensated sonar system may be used to estimate the transfer function of a target, $H_{ST}(\omega)$, via the frequency domain operation

$$H_{TS}(\omega) = \frac{S_{RX}(\omega)}{S_{TX}(\omega)}. \quad (7)$$

Parameters such as $H_{TS}(\omega)$ are complex valued and thus contain the equivalent of magnitude and phase information. A fully corrected system is assumed to have been compensated for both magnitude and phase response, whilst a partially corrected system may have been corrected for magnitude response only.

It is likely that a discrete, numerical representation of the above quantities will be used. Thus, if the signals are sampled at a rate of f_s samples per second, the continuous form of a signal such as the transmit signal waveform, $s_{TX}(t)$, may be represented by a discrete version, $s_{TX}(k)$. The integer index, k, may take any value between zero and $N-1$, where N is the number of samples in a data block, or snapshot, being processed. In many cases, a number of snapshots, M, will be averaged to reduce the variance of the estimated parameter. The discrete time domain signal, $s(k)$, may be transformed to the frequency domain, $S(n)$, using the discrete Fourier transform

$$s(k) \leftrightarrow S(n)$$

$$S(n) = \sum_{k=0}^{N-1} s(k) \exp\left(-2\pi i k n / N\right) \quad (8)$$

$$s(k) = \frac{1}{N} \sum_{n=0}^{N-1} S(n) \exp\left(2\pi i k n / N\right)$$

Where $i = \sqrt{-1}$ and the integer index, n, may take any value between zero and $N-1$. When performing circular convolution and correlation operations, the discrete time domain signal, $s(k)$, may have to be zero-padded by concatenating additional samples set to zero to increase the length of the original data snapshot.

III. Measurement Workflow

A typical compensation estimation workflow chain may take the form shown in Fig. 2. This comprises an estimation of the ambient noise level (III.A), an estimate of the clutter level without and then with a standard target being present (III.B), the selection of a suitable transmission signal for use during the correction factor estimation process (III.C), a measurement of the sonar system response with the standard target present (III.D) and an estimate of the quality metrics (III.E). On completion of this workflow, a fully corrected sonar system should be available for measuring the target strength and possibly an estimate of the transfer function of a variety of acoustic scatterers.

Given no *a priori* knowledge of the transmit and receive correction functions, $h_{TX}(k)$ and $h_{RX}(k)$, these will often be initially set to impulse functions

$$\begin{aligned} h_{TX}(k) = h_{RX}(k) = 1 \quad \text{for} \quad k = 0 \\ h_{TX}(k) = h_{RX}(k) = 0 \quad \text{otherwise} \end{aligned} \tag{9}$$

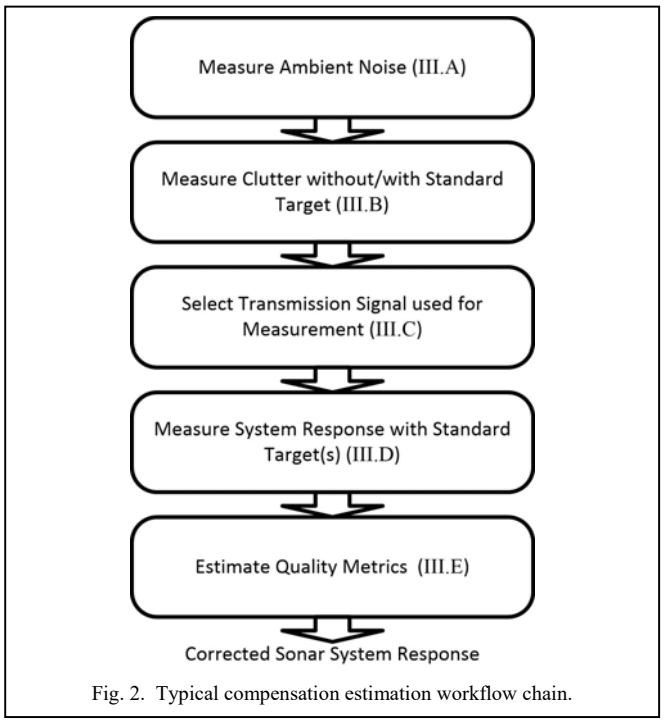

Fig. 2. Typical compensation estimation workflow chain.

A. Ambient Noise Level Estimation

An estimate of the mean-squared ambient noise level, $S_{AMB}(n)$, will be made over M data snapshots with no transmission active ($s_{TX}(k) = 0 \quad \text{for all} \quad k$) and appropriately normalized to a 1 Hz bandwidth. This procedure is known as Welch's method, or the periodogram method, for estimating ambient noise power spectra.

This value is usually normalized by the equivalent noise bandwidth to provide spectral levels measured in units of $dB\ re\ 1W\ Hz^{-1}$, or $dB\ re\ 1\mu Pa^2\ Hz^{-1}$ assuming that the sensitivity of the hydrophone is known. The periodogram of a block of the m^{th} block of N samples is defined as:

$$P_{AMB}(m,n) = \frac{1}{N}\left|S_{RX}(n)\right|^2 = \frac{1}{N}\left|\sum_{k=0}^{N-1} s_{RX}(k)\exp\left(-2\pi ikn/N\right)\right|^2 \tag{10}$$

The Welch estimate is then obtained by averaging over the M data snapshots.

$$S_{AMB}(n) = \frac{1}{M}\sum_{m=0}^{M-1} P_{AMB}(m,n) \quad . \tag{11}$$

This quantity provides a baseline measure for use during the transmit signal selection process. The discrete mean squared ambient noise level may also be estimated by applying Parseval's theorem, assuming a discrete Fourier Transform of length N has been applied. This may be used where a single measure is required for the noise level rather than a spectrum.

$$\frac{1}{N}\sum_{n=0}^{N-1}\left|S_{RX}(n)\right|^2 = \sum_{k=0}^{N-1}\left|s_{RX}(k)\right|^2 \tag{12}$$

B. Clutter Level Estimation

An estimation of the clutter level (unwanted large-amplitude scattering sources) will be made both without and with a standard target present, in order to determine the signal-to-clutter ratio. For this purpose, a transmission signal, $s_{TX}(k)$, with good range resolution and low range-sidelobes will be adopted. Typical examples include pulsed sinusoidal transmissions with a short pulse duration of k_p samples.

$$\begin{aligned} s_{TX}(k) &= \Im\left\{\exp\left(i2\pi fk/f_s\right)\right\} \quad \text{for} \quad 0 \le k \le k_p \\ s_{TX}(k) &= 0 \quad \text{otherwise} \end{aligned} \tag{13}$$

and the Richer wavelet (for ultra-wideband systems)

$$s_{TX}(t) = \left(1 - \frac{k^2}{\sigma^2 f_s^2}\right)\exp\left(\frac{-k^2}{2\sigma^2 f_s^2}\right) \quad \text{for} \quad -k_p \le k \le k_p \tag{14}$$

where σ is a parameter related to the width of the main lobe, with typically $\sigma = k_p \big/ 4 f_s$.

The purpose is to identify periods of the received signal with minimal clutter. A schematic measurement environment and associated impulse response is illustrated in Fig. 3. The standard target will be mounted using a minimally invasive support mechanism as far away from the sonar system as is practical. The dimensions of all environments are likely to be limited by boundary conditions such as tank walls or the hull of a vessel.

In many circumstances, it is difficult to unambiguously identify the echo response associated with the standard target. Thus common practice is to ensonify the measurement environment without the standard target present and then to ensonify the environment with the standard target present. The difference in temporal responses helps identify the contribution of the standard target.

For illustrative purposes, Fig. 3 includes a projector-target-hydrophone path 1, a projector-surface-target-hydrophone path 2, a projector-bottom-target-hydrophone path 3 and projector-boundary-hydrophone paths 4,5. The transmission origin is identified as $k = 0$, the occurrence of the projector-target-hydrophone path is identified as k_1 and the next clutter response is identified as k_2. The temporal measurement window used for all subsequent measurements will start at k_1 and terminate at k_2. It is normally desirable to maximize the duration of the measurement window by careful placement of the sonar system and standard target with respect to the boundaries, as the duration of the transmission signal, $s_{TX}(k)$, is usually set to equal this measurement window. Increased transmission signal durations are generally linked to improved signal-to-noise ratio measurements and improved spectral resolution.

The clutter associated with a laboratory tank is readily computed using the image source method [4]. A Dantzig simplex algorithm may then be applied to optimize the temporal separation between clutter returns using fixed constraints of the measurement tank boundaries and six free-variables associated with the positions of the transducer and standard target.

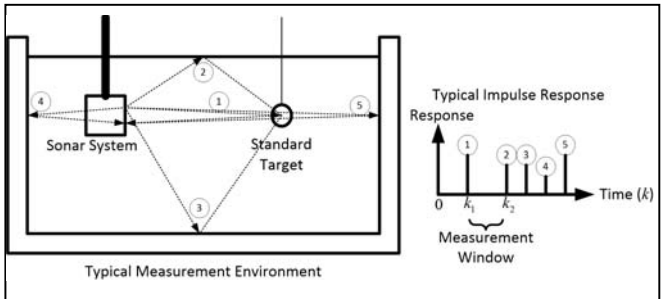

Fig. 3. Schematic diagram of a representative tank-based measurement environment

A mean square estimate of the clutter plus ambient noise, n_{CPN}, is obtained over the M data snapshots from

$$n_{CPN} = \frac{1}{M}\sum_{m=0}^{M-1}\left(\frac{1}{(k_2 - k_1 + 1)}\sum_{k=k_1}^{k_2}\left|s_{RX}(m,k)\right|^2\right). \qquad (15)$$

The parameter, n_{CPN}, is a key parameter used within the quality metrics.

C. Choice of Transmission Signal

A transmission signal should now be selected such that the echo from the standard target will start at k_1 and terminate at k_2, implying range-gating as an aid to clutter reduction. Thus, the pulse duration will become $k_p = k_2 - k_1 + 1$, whilst any echo lengthening caused by the standard target is neglected. Typical examples of signals used in this part of the workflow include pulsed sinusoidal transmissions and the linear frequency modulated pulse.

The most commonly encountered measurement signal in stable environments, such as a land-based tank, is that of a stepped-frequency pulsed sinusoid. A range of frequencies is selected where useful energy may be projected by the system. The lower band edge is denoted by f_1 and the upper band edge is denoted by f_2. The step increment is often set to half the theoretical resolution based on the need for zero-padding of the time domain output. Thus, the step increment is $f_s/(2k_p)$.

The notional pulse duration is k_p samples. This is usually modified to a new value, k_{pm}, such that an integer number of cycles is transmitted and that the time domain signal starts and terminates at a zero-crossing point. Thus, if the frequency to be projected is f, the modulus of k_{pm} and f_s/f should be zero. The transmission waveform may be described by

$$\begin{aligned} s_{TX}(k) &= \Im\left\{\exp\left(i2\pi fk/f_s\right)\right\} \quad \text{for} \quad 0 \le k \le k_{pm} \\ s_{TX}(k) &= 0 \quad \text{otherwise} \end{aligned} \qquad (16)$$

The advantages of a stepped-frequency pulsed sinusoid are that the highest signal-to-noise and spectral resolution may be obtained. The disadvantages are that of long data collection periods as only one frequency may be estimated per ping and that a very stable measurement environment is required.

Any modulated signal that projects a range of frequencies within a limited pulse duration may also be employed. However, the linear frequency modulated pulse is most commonly encountered as the spectral content tends towards a uniform distribution. The transmission waveform may be described by

$$s_{TX}(k) = \Im\left\{\exp\left(i2\pi f_1 k / f_s + i\pi B k^2 / \left(k_p f_s\right)\right)\right\} \quad \text{for} \quad 0 \le k \le k_p \qquad (17)$$
$$s_{TX}(k) = 0 \quad \text{otherwise}$$

Where the bandwidth is $B = f_2 - f_1$. The linear frequency modulated pulse sweeps from frequency f_1 to a frequency $f_1 + B$ in a time corresponding to k_p samples. The bandwidth is often adjusted so that the time domain signal starts and terminates at a zero-crossing point.

D. Measurement of the Sonar System Response with the Standard Target present

The measurement workflow continues by ensonifying the standard target and estimating the spectrum of the received signal, $S_{RX}(n)$. The signal-to-noise ratio of the measurement is usually optimized via the use of a matched filter. Assuming that the ambient noise spectrum obtained in III.A was substantially flat, this process may be replaced by the biased replica correlation operation to obtain a time domain estimate, $s_{RXMF}(k)$.

$$s_{RXMF}(k) = \sum_{l=0}^{N-k-1} s_{RX}(l) s_{TX}(l+k) \quad \text{for} \quad 0 \le k \le \left(N - k_p\right) \qquad (18)$$

The replica correlation operation is usually performed in the frequency domain, this also yielding the cross-spectrum.

$$s_{RXMF}\left(k\right) \leftrightarrow S_{RX}\left(n\right) S_{TX}^{*}\left(n\right) \qquad (19)$$

The estimate of the cross-spectrum, $S_{CS}\left(n\right)$, is smoothed by coherent averaging over a number of pings

$$S_{CS}\left(n\right) = \frac{1}{M} \sum_{m=0}^{M-1} S_{RX}\left(m,n\right) S_{TX}^{*}\left(m,n\right) \qquad (20)$$

For the case of a stepped-frequency pulsed sinusoid transmission a single complex value will be extracted from S_{CS} corresponding to the center frequency of the transmission. Where a modulated transmission signal has been employed, multiple complex values will be extracted from $S_{CS}\left(n\right)$.

For the purposes of deriving the correction factors defined in (3), an additional replica correlator has been implemented for use during the measurement process. Thus, some values from $S_{CS}\left(n\right)$ will be employed to form part of $S_{RX}\left(n\right)$ determined by the choice of transmission signal. The process will be repeated using different transmission signals until $S_{RX}\left(n\right)$ is appropriately populated, based on the choice of quality metric discussed in section III.E.

E. Determination of Quality Metrics

A vector diagram representation of the received signal and noise components is shown in Fig. 4. A snapshot of the desired time domain signal vector, $s_{SIG}(t)$, is illustrated as a reference component orientated in the vertical direction. The interfering components associated with noise and clutter are assumed to be non-deterministic, thus resulting in a component, $s_N(t)$, that has a phase angle that is uniformly distributed over 2π radians. This may be modelled by the combination of an in-phase vector, $s_{NI}(t)$, and a quadrature vector, $s_{NQ}(t)$. The resultant received signal, $s_{RES}(t)$, will thus have an amplitude that differs from the desired signal vector, $s_{SIG}(t)$, and a phase angle that differs by a value, ϕ .

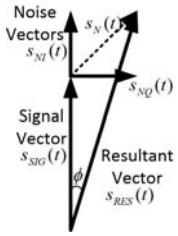

Fig. 4. Vector diagram representation of received signal and noise components

An estimate of the noise and clutter signal was obtained in section III.B. The sampled version of the mean squared values of $s_N(t)$, was computed as N_{CPN} within a carefully selected time-gated window starting at sample k_1 and ending at sample k_2.

Similarly, an estimate of the signal-plus-noise value in the same time-gated window was obtained in section III.D. The sampled version of the mean squared values of $s_{RES}(t)$, was computed as $s_{RXMF}\left(k\right)$, or as a smoothed estimate of the cross-spectrum, $S_{CS}\left(n\right)$, in (20).

The signal-plus-noise-to-noise ratio, s_{SPNNR}, is

$$s_{SPNNR} = \frac{s_{RXMF}}{n_{CPN}} = s_{SNR} + 1 \qquad (21)$$

The efficacy of a system correction operation may be defined in terms of the difference in levels of the mean squared signal and the mean squared signal plus noise, ΔL_{SPNN} . This is related to the required signal-to-noise ratio level, L_{SNR}, by

$$L_{SNR} = 10\log_{10}\left(\frac{10^{\Delta L_{SPNN}}}{1 - 10^{\Delta L_{SPNN}}}\right) \qquad (22)$$

Or the required signal-plus-noise-to-noise ratio level, L_{SPNN}, by

$$L_{SPNN} = 10\log_{10}\left(1+\frac{10^{\Delta L_{SPNN}}}{1-10^{\Delta L_{SPNN}}}\right) \quad (23)$$

Typical examples encountered during a measurement flow process would be that of a desired modulus error ΔL_{SPNN} of 0.1 dB requiring a signal-plus-noise-to-noise ratio, L_{SPNN} of 16.4 dB. Relaxing ΔL_{SPNN} to a value of 1 dB reduces the value of L_{SPNN} to 6.9 dB.

Examining the vector diagram shown in Fig. 4 yields an approach for determining the phase error ϕ.

$$\phi = \tan^{-1}\left(\frac{s_{NQ}}{s_{SIG}+s_{NI}}\right) \quad (24)$$

For large values of signal-to-noise ratio, s_{SIG}/s_{NI}, this may be approximated by

$$\phi \approx \left(\frac{s_{NQ}}{s_{SIG}}\right) \quad (25)$$

This approximation is useful for phase errors of less than 8°, corresponding to signal-to-noise ratios of greater than 14 dB. A frequently encountered commercial specification is that of measuring the phase response within a multi-element array to better than 5°, thus requiring a signal-plus-noise-to-noise ratio, L_{SPNN} of 18.4 dB.

The correction process is designed to determine complex values for $H_{TXRX}(\omega) = H_{TX}(\omega)\,H_{RX}(\omega)$ over a limited frequency range. A number of the spectra obtained during an indicative measurement process are illustrated in Fig. 5.

The lower, solid, black line that decreases with frequency is indicative of the environmental noise and clutter estimated in section III.B.

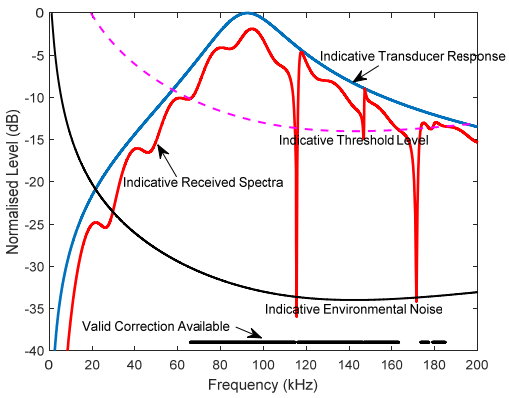

Fig. 5. Indicative environmental noise, received signal and correction response measurement spectra with y-axis normalised to the peak transducer response

The minimum signal-to-noise ratio required to estimate a compensation function has been shown in section III.E to typically be in the range 10 dB to 20 dB. This is illustrated as a magenta, dashed line labelled 'Indicative Threshold Level'.

The 'Indicative Received Signal' obtained in section III.D is shown as a solid, red line. This will approximately follow the form of the 'Indicative Transducer Response', but perturbations and deep nulls may be present as a result of the characteristics of the standard target.

Wherever the 'Indicative Received Signal' exceeds the 'Indicative Threshold Level', a 'Valid Correction Available' state may be achieved. For the example shown in Fig. 4, four separate correction bands are observable.

Ideally, a single contiguous correction band is required. Possible improvements may be achieved by:

- In an ambient noise limited case, increasing the transmit power, or reducing the noise level by baffling the environment with acoustic absorbers.
- In a clutter limited case, modifying the range gating extents discussed in III.C, altering the standard target geometry, or by placing absorbers around the boundaries of the environment.
- In a standard target limited case, substituting a standard target such that any spectral nulls are outside the frequency band of interest.
- In a standard target limited case, substituting a number of standard targets and performing a weighted average of the resulting correction factors.

The correction function is likely to be discontinuous, or include abrupt transitions as illustrated in Fig. 6.

The correction level will generally assume a value of minus infinity, corresponding to a field value of zero, in regions where an inadequate signal-plus-noise-to-noise ratio is available. An alternative, as illustrated in Fig. 6, is to set the correction level to an appropriate small constant value.

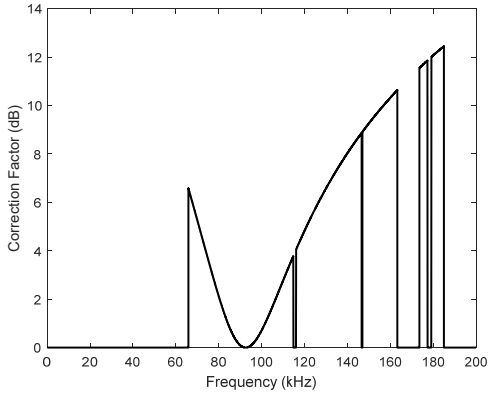

Fig. 6. Indicative correction factor

In both cases, a spectral widowing function will be required if the spectrum is to be transformed back to the time domain, thus reducing the effects of step-function changes in the correction factor. Of interest for this purpose is the Tukey, or tapered cosine, window function operating over a modified pulse duration of k_{pm} samples, such that an integer number of cycles is transmitted and that the time domain signal starts and terminates at a zero-crossing point. This taper function is used to ramp-up and ramp-down the amplitude of the transmission signal over k_{Tuk} samples whilst reducing spectral leakage.

$$w(k) = \frac{1}{2}\left(1+\cos\left(\frac{\pi k}{k_{Tuk}} - \pi\right)\right) \qquad 0 \le k < k_{Tuk}$$
$$w(k) = 1 \qquad k_{Tuk} \le k \le k_{pm} - 1 - k_{Tuk}$$
$$w(x) = \frac{1}{2}\left(1+\cos\left(\frac{\pi\left(k - k_{pm} + 1\right)}{k_{Tuk}} + \pi\right)\right) \qquad k_{pm} - 1 - k_{Tuk} < k \le k_{pm} - 1 \tag{26}$$

Typically, the ramp-up and ramp-down durations are of the same order as the transient duration of the transducer. Thus, a transducer of resonant frequency f_0 with a Q-factor q operating in a system with sampling frequency f_s might imply that $k_{Tuk} = \dfrac{q\ f_s}{f_0}$.

Frequently encountered alternatives to the tapered cosine window include linear ramp functions.

IV. TRANSMISSION LOSS

The acoustic signal is subjected to a two-way transmission loss, $h_{2TL}(t)$, and the echo formation process resulting from the interaction with a standard target, $h_{ST}(t)$. These factors must be incorporated within the correction process.

The two-way transmission loss, $h_{2TL}(t)h_{ST}(t)$, is generally assumed to comprise a geometrical spreading component and an absorption component. For standard targets of finite dimensions, square-law spreading is assumed of the form

$$H_{2TL} = 40\log_{10}(r) \tag{27}$$

where r is the range between the phase center of a monostatic sonar system transducer and the center of the standard target.

For the case of a continuous standard target, such as the surface of a large laboratory tank, the geometrical spreading law is equivalently

$$H_{2TL} = 20\log_{10}(2r) \tag{28}$$

where r is the range between the phase center of a monostatic sonar system transducer and the continuous surface.

The absorption, or medium correction factor is generally computed from published models. The formulations of Francois and Garrison (1982), ANSI/ASA S1.20-2012 Annex B are applied.

The standard target is normally assumed to be located within the far field of the transducer and vice versa. One common assumption is that far field conditions may be assumed at a Fresnel distance of a^2/λ, where a is the radius of a circular transducer, or spherical target. Should a simple spherical spreading model be assumed, then an error of 0.41 dB would be incurred if the target were located on-axis at three times this assumed far field range. A spherical target of the same size as the transducer would double this error to 0.82 dB. Operating ranges in excess of ten times the assumed far field range transition are preferred.

Ideally, a full field propagation model should be computed for all situations [5].

V. MEASUREMENTS

The measurements presented within this paper were made with a representative broadband transducer containing a 50 mm disc of 1-3 composite ceramic elements with center frequency of 500 kHz (type 6050B). This transducer was manufactured by Neptune Sonar Limited, Kelk, United Kingdom and has a beamwidth of the order of 3.5 degrees at the nominal operating frequency

The equivalent circuit model was determined over the frequency band determined by the -3 dB band (half-conductance values). A least-mean-square fit was employed to derive the equivalent model illustrated in Fig. 7.

For transmit purposes, matching circuitry was added to implement a second order Bessel bandpass response. This comprised a parallel shunt inductance of 56.7 micro henrys and a series resistance of 252 ohms. A network synthesis approach was implemented to optimize bandwidth at the expense of power dissipation [6]. Optimizing bandwidth results in using the minimal number of passive components within the matching circuitry. Broadband harmonic suppression levels of -100 dB were targeted for this application and inductors wound on ferrite cores were found to be unable to meet this specification. Thus large, air-cored inductors were specially manufactured for the matching circuitry.

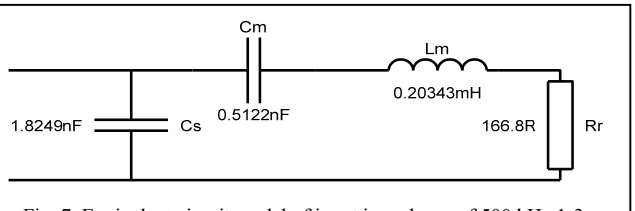

Fig. 7. Equivalent circuit model of input impedance of 500 kHz 1-3 composite TX transducer

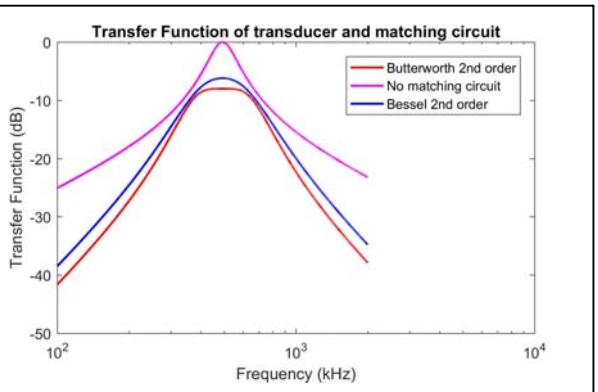

Fig. 8. Modulus transmit transfer response of 500 kHz 1-3 composite transducer

The modelled modulus transmission transfer response of the transducer and matching circuit is shown in Fig. 8. The result of connecting the transducer directly to the power amplifier is displayed as a reference for the second order Butterworth and Bessel matching circuits – although many power amplifiers would be unstable driving such a reactive load.

The phase of the transmit transfer response of the transducer and matching circuit is shown in Fig. 9 for a second order Bessel implementation. A linear phase response is maintained to at least the -10 dB response points – this being of critical importance where time-domain signal fidelity is required.

A. Acoustic Measurements from a Planar Surface

It is desired to establish the transfer function of the standard target, $H_{TS}(\omega)$, using a total system correction approach. However, this implies that an ideal reference target is available with precisely known and stationary characteristics. One possible candidate is that of a continuous pressure release boundary approximated by a perfectly smooth water surface. Such approaches have been used for the self-reciprocity calibration of low frequency transducers [7,8].

The transducer was bottom-mounted on a two-axes pan-and-tilt unit and scanned for maximum response from the surface. The pan-and-tilt units had an angular resolution of 0.1 degrees and backlash effects were minimized by always rotating in the same direction. The dimensions of the laboratory water tank at the University of Birmingham were 8.48 m in length, 3.95 m in width, and 3.04 m in depth.

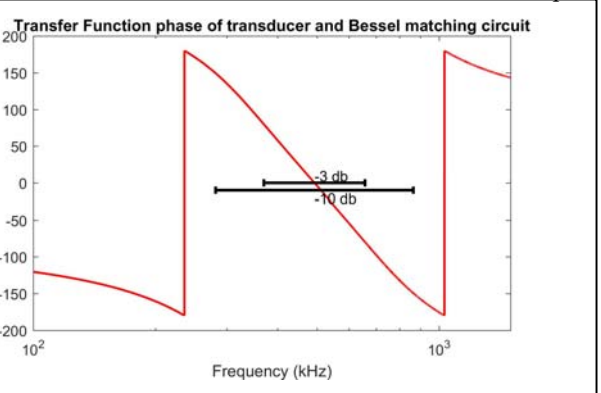

Fig. 9. Phase of transmit transfer response of 500 kHz 1-3 composite transducer

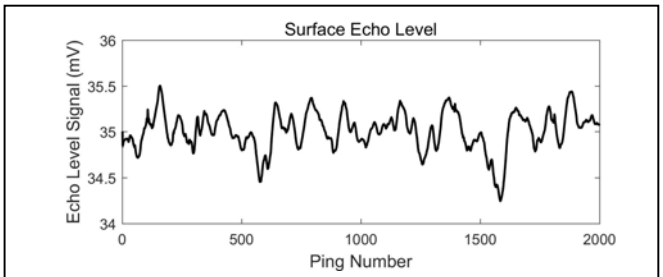

Fig. 10. Typical result of 2000 surface reflection pings in a laboratory tank

A typical result for 2000 consecutive pings transmitted within a laboratory tank is shown in Fig. 10. If the variance of the surface Echo Level is assumed to be a noise source within the correction process, then the SNR for this data is 44 dB, thus contributing an insignificant error. It will be noted that the variance appears to have some periodic content.

The variance of surface Echo Level was observed to be related to disturbances of the surface of the tank – exponentially decaying over a period of days following any changes in the deployment of the transducer. Thus, a surface height probe was deployed consisting of a Micro-Epsilon ILD1420-50 laser measurement displacement sensor. This device had a spot size on the surface of approximately 250 μm, a height repeatability of 2 μm and a sampling rate of 2 kHz. Fine pepper dust was dispersed onto the surface to provide an optical scattering interface.

A representative surface displacement result is shown in Fig. 11. This shows longer-term displacements believed due to thermal variations within the laboratory. The impulse is due to a pressure wave of a door being opened and closed. The finer structure is the wave motion of the surface of the tank.

Computing the power spectral density of the laser height measurements reveals the results shown in Fig. 12. The spectrum is dominated by a component at 0.275 Hz which is consistent with the dimensions of the tank, with a level of 1.37×10^{-5} mm^2.

Analytic derivations exist for the acoustic scattering from corrugated surfaces [9] and for the degradation in array gain in towed arrays [10, 11]. In this case, a numerical estimation of the equivalent target strength reduction was performed and was in good agreement with the variance obtained from the acoustic measurements of the surface.

Thus, it is believed that laser measurements of the water surface displacement can predict the uncertainty of the acoustic measurements using the surface as a standard target. The acoustic measurements need only be commenced after the surface amplitude variations have reduced to below a pre-determined value. This procedure showed that the efficacy of

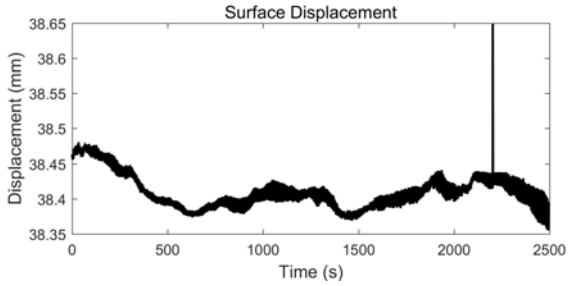

Fig. 11. Typical surface displacement measured using a laser sensor

acoustic measurements were primarily affected by re-arranging

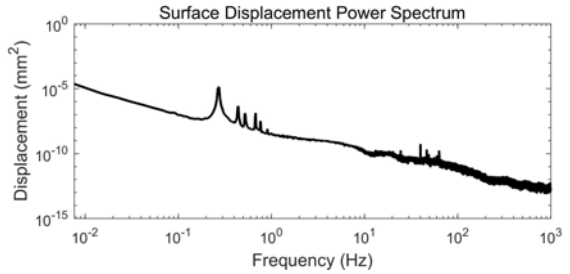

Fig. 12. Typical power spectral density of surface displacement

of cables and anything else entering the water, less effected by air currents and no statistical link was established with local heavy traffic.

Having established that a sufficiently smooth water surface existed, a frequency transfer function was estimated. This comprised a 1 ms transmission pulse in order to avoid boundary clutter, with a transmission stepping from 200 kHz to 1 MHz in 1 kHz increments. A typical Echo Level is shown in Fig. 13, this being in close agreement to the modelled second order Bessel transfer function shown in Fig. 7.

The correction factor, $H_{TXRX}(\omega)$, can now be computed and applied to measurements of other standard targets. The results of ambient noise and clutter measurements indicates that a usable frequency range over which correction may be applied is 250 kHz to 800 kHz for this sonar system.

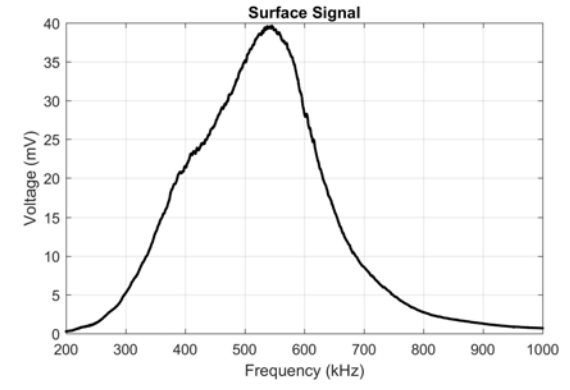

Fig. 13. Measured Echo Level when using the surface as a standard target

B. Acoustic Measurements from Spherical Standard Targets

The monostatic transducer and standard target were placed within the measurement tank in accordance with the procedures outlined in section III.B. The transmission pulse duration was reduced to 0.2 ms to avoid clutter and the step frequency was increased to 5 kHz.

Spherical standard targets of diameter 100 mm were deployed using a Kevlar suspension net. The first sphere was maneuvered into the peak of the beam response using an XZ table mounted above the surface of the tank. Thereafter, the same suspension net was used for the remaining spheres in the belief that sub-millimetric position repeatability could be obtained. Operating frequencies of between 250 kHz and 800 kHz represent high *ka* value regions and so the target strength (TS) contains significant structure and variability between standard target. This is illustrated in Fig. 14 where the target strength results from three spheres are overlaid.

The variation between standard target may be quantified by computing the standard deviation-to-mean ratio. This is illustrated in Fig, 15 and shows that this metric has a low value wherever there is a deep null in the response of the target strength spectra. This is partially due to uncertainties in material properties and partially due to reduced signal-to-noise ratio during the measurement process.

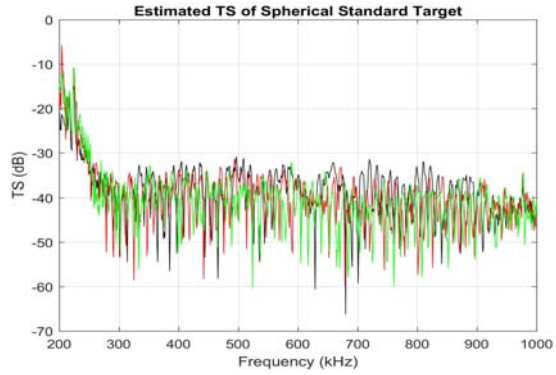

Fig. 14. Measured Target Strength (TS) of three, 100 mm diameter standard targets

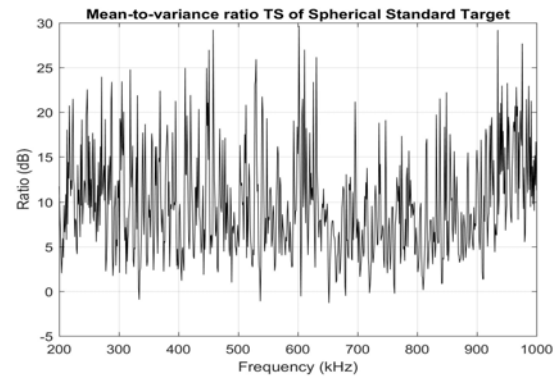

Fig. 15. Measured Target Strength (TS) of three, 100 mm diameter standard targets

VI. CONCLUSIONS

The processes required for comparing a range of standard targets have been presented. In this case, the reference standard target was that of the air-water interface of a laboratory tank. Any deviation from a planar surface introduces significant uncertainty in the computation of the combined sonar system correction function. A laser displacement probe was used to determine when acoustic measurements could be made to a given level of repeatability.

A production batch of low-cost aluminum spherical standard targets were then compared and statistical metrics derived as a function of frequency to aid the production processes.

ACKNOWLEDGMENT

The authors wish to thank Subsea Asset Location Technologies (SALT) Ltd, Dorset, United Kingdom for manufacturing a range of aluminum standard targets from a variety of billets used in the measurements presented within this paper. This work was partially funded by Innovate UK, Project reference 132403..

REFERENCES

[1] D. Stansfield, “Underwater Electroacoustic Transducers,” Bath University Press and Institute of Acoustics, Bath, UK, 1991.

[2] K.G. Foote, “Optimizing copper spheres for precision calibration of hydroacoustic equipment,” The Journal of the Acoustical Society of America 71, 742 (1982).

[3] T.K. Stanton, D Chu, “Calibration of broadband active acoustic systems using a single standard spherical target,” The Journal of the Acoustical Society of America 124, 128 (2008).

[4] J.B. Allen, and D.A. Berkley, “Image method for efficient simulating smallroom acoustics,” Journal of the Acoustical Society of America, 65, no 4, pp. 943- 950 (1979).

[5] K. G. Foote, “Discriminating between the nearfield and the farfield of acoustic transducers,” J. Acoust. Soc. Am., 136, 1511-1517 (2014).

[6] R. Raut and M. N. S. Swamy, “Modern Analog Filter Analysis and Design,” Wiley-VCH (2010), ISBN 10: 3527407669

[7] R.B. Patterson, “Using the Ocean Surface as a Reflector for a Self-Reciprocity Calibration of a Transducer,” The Journal of the Acoustical Society of America 42, 653 (1967).

[8] R.J Bobber, "Underwater Electroacoustic Measurements," Naval Research Laboratory, Washington D.C., 1970.

[9] E.O. LaCasce, and P. Tamarkin, “Underwater sound reflection from a corrugated surface,” Journal of Applied Physics, 27: 138–148. 1956.

[10] D.M. Caveny, D.R. Del Balzo, J.H. Leclere, “Performance of sinusoidally deformed hydrophone line arrays,” The Journal of the Acoustical Society of America 105.4 (1999): 2203-2209.

[11] M. J.Hinich, and W.Rule, “Bearing estimation using a large towed array,” Journal of the Acoustical Society of America, 58(5), 1023-1029. 1975.